Effect of Intermolecular Electrostatic Interactions on the End-over-End Rotational Dynamics of 200-Base-Pair DNAs

Alexei N. Naimushin, Bryant S. Fujimoto, and J. Michael Schurr*

Department of Chemistry, Campus Box 351700, University of Washington, Seattle, Washington 98195-1700

Received May 3, 1999; Revised Manuscript Received August 23, 1999

ABSTRACT: The *self*-rotational diffusion coefficients (D_R) of 200 bp DNAs were measured by a new transient polarization grating method. Measurements were performed over a range of added ionic strengths from 4 to 47 mM at a DNA concentration of 1.5 g/L, where the prevailing intermolecular electrostatic interactions begin to significantly affect the *self*-rotational relaxation times ($\tau_R \equiv (6D_R)^{-1}$). With decreasing added ionic strength from 20 to 4 mM, τ_R is observed to increase by 12% from 3800 to 4260 ns. Abolition of this increase, when the DNA concentration is reduced by 2-fold to 0.75 g/L, demonstrates the *inter*molecular origin of this phenomenon. The strengths of the intermolecular interactions are characterized by the second virial term, ρB_2, where ρ is the DNA rod density and B_2 is the second virial coefficient. This second virial term takes the values 0.27, 0.37, 0.46, and 1.53 at respectively 47, 26, 20, and 4 mM added ionic strength. The rise in τ_R between 20 and 4 mM added ionic strength is associated with a large increase in the second (and third) virial terms that reflects a shift from primarily two-rod to multirod interactions. A theory is formulated for the enhancement of rotational friction via reflected hydrodynamic interactions from the neighbors around a given diffusor. The increase in τ_R with decreasing added ionic strength from 20 to 4 mM is attributed to increasingly parallel alignment of neighboring rods over this range. Because perpendicular orientations are favored when two-rod interactions dominate the virial series, it is inferred that parallel orientations must be favored by multirod interactions. According to the second virial terms, the rise in τ_R of the present 200 bp DNA sample on one hand and the decrease in scattered intensity and change in translational dynamics of the 150 bp DNA sample studied by Fulmer et al. on the other appear to occur over similar ranges of corresponding states. These intermolecular structural transitions evidently are not true isotropic to nematic transitions but may correspond to a thwarted transition of that kind.

Introduction

Under low salt conditions, long-range electrostatic interactions between dilute polyelectrolytes profoundly affect their equilibrium spatial correlations and translational diffusion dynamics.[1,2] For example, as the salt concentration of a 1.5 g/L solution of ∼150 bp DNA is decreased from 16 to 5 mM, the intensity of scattered light decreases by 1.9-fold, the rate of ordinary translational diffusion increases substantially, and a second extraordinarily slow diffusive component appears in the dynamic light scattering (DLS) correlation functions.[3] This behavior is similar to the ordinary−extraordinary (OE) transition reported for flexible polyelectrolytes,[1,2] although the salt concentration at which it occurs is about 20-fold higher than would be expected for a flexible polyion.[4] This difference might arise from the much longer persistence length of the DNA, which may promote significant *orientational* as well as translational ordering at a higher salt concentration than where the OE transition would otherwise occur. If orientational ordering plays a significant role in this transition, then one would expect a significant effect of both salt and DNA concentration on the end-over-end rotational dynamics of the DNA.

Our goal here is to assess the effects of *intermolecular* electrostatic interactions on the end-over-end rotational diffusion of 200 bp DNAs, as the salt concentration is varied through the region where substantial changes in spatial pair correlations and translational dynamics are known to occur. With increasing concentration of rodlike polymers, their rotational diffusion is expected to become significantly hindered by caging only when $c_pL^3 \gtrsim 50$, where c_p and L are the rod concentration and length, respectively.[5,6] For 200 bp DNAs at 1.5 g/L, one has $c_pL^3 \cong 2$, so simple caging effects *due to hard-cylinder interactions* are *not* expected. However, changes in strength of hydrodynamic interactions with changing orientational and spatial pair correlations *can* significantly affect the rate of rotational diffusion, as will be demonstrated.

Some evidence for a reduced rate of rotation of a flexible polyion, polystyrenesulfonate, in the low-salt extraordinary regime comes from NMR quadrupolar relaxation studies of the $^{23}Na^+$ counterions.[7] However, in the case of a flexible polyion, it is difficult to separate intramolecular effects, such as polyion extension, from intermolecular effects, such as induced parallel orientational order, either of which could decrease the rate of rotational diffusion. A small dip in the intrinsic viscosity of poly(L-lysine) with decreasing salt concentration at the OE transition may reflect the onset of some parallel ordering of neighboring chains or sections of chains.[8] Apart from these measurements, virtually nothing is known about changes in rotational dynamics and orientation pair correlations in the transition region. Measurements of the self-rotational diffusion coefficient of DNA molecules with decreasing ionic strength through this transition region in principle allow a qualitative assessment of whether orientational

* Corresponding author. Tel (206) 543-6681; FAX (206) 685-8665; e-mail schurr@chem.washington.edu.

10.1021/ma990690v CCC: $18.00
Published on Web 11/10/1999

ordering occurs and whether the intermolecular electrostatic interactions promote parallel or perpendicular alignment of neighboring rods.

The self-rotational diffusion coefficient of 200 bp DNAs is measured at a DNA concentration of 1.5 g/L in solutions of various ionic strengths, namely 4, 8, 14, 20, 26, and 47 mM, and also at a DNA concentration of 0.75 g/L in 4 mM ionic strength. These measurements were performed via a new transient polarization grating (TPG) experiment that is described briefly under Materials and Methods. Evidence that increasing strength of *intermolecular* electrostatic interactions leads to a decrease in rotational diffusion coefficient and the resulting implications of that for intermolecular orientational pair correlations are described under Results and Discussion.

Materials and Methods

The Sample. The sample of 200 bp DNA was prepared by copying the sequence from position 233 to 432 of pBR322 by polymerase chain reaction (PCR). This sequence contains 56% GC composition. Details of the sample preparation, purification, and characterization are presented elsewhere.[9] The purification protocol includes (1) protein digestion by proteinase K and removal of the products by multiple extractions with buffered phenol; (2) exhaustive dialysis alternately vs high salt (HSTE) (500 mM NaCl, 10 mM Tris, 1 mM Na_2EDTA, pH 8.5, at 21 °C) and normal salt (NSTE) (100 mM NaCl, 10 mM Tris, 1 mM EDTA, pH 8.5 at 21 °C) buffers at 4 °C, terminating finally in the latter; and (3) hydroxyapatite chromatography. The sample characterization includes (1) confirmation of the sequence by direct sequencing and (2) gel electrophoretic comparison with standards of known length to certify that the tertiary structure is normal. By all criteria, including gel electrophoresis, our 200 bp DNA sample is completely monodisperse. For optical anisotropy studies, the samples contain either 1.5 g/L DNA (i.e., 1.13×10^{-5} M DNA molecules or 2.3 mM base pairs) or 0.75 g/L DNA. The lowest ionic strength (4 mM) buffer contains 5 mM Tris, pH 7.5. All higher ionic strength (8, 14, 20, 26, and 47 mM) buffers contain 10 mM Tris, pH 7.5, plus various concentrations of added NaCl. DNA concentrations are determined from the UV spectrum of an appropriately diluted sample by assuming that $A_{260} \cong 1.0$ for a 0.05 g/L solution. The samples also contain added methylene blue (MB) at a concentration of 1 dye/100 bp. Intercalated MB serves as the extrinsic optical probe in our experiments. The MB was purified as described.[10]

The binding constant of MB for a single intercalation site at 20 °C in 4 mM ionic strength was estimated from the data of Hagmar et al.[11] in the manner described earlier[12] and found to be 1.9×10^5 M^{-1}. Under the conditions prevailing in our 4 mM ionic strength sample, the MB is practically all (99.8%) bound. However, as shown previously,[12] even under low ionic strength conditions, MB occupies (at least) three different intercalation sites with similar unwinding angles, but very different fluorescence lifetimes (25, 130, and 620 ps). The transient photobleaching (due to triplet formation) was found to arise predominantly from the longest-lived of these intercalated species, which was associated with AT, TA, or AA steps.[12] These sites account for most of the transient photobleaching in the present experiments. At 4 mM ionic strength, these sites comprise only about 20% of the total bound dye, the remainder of which is comparatively silent in our experiments. From the fluorescence lifetimes and relative fluorescence amplitudes, we estimate that the longest-lived sites are responsible for about 75% of the total observed photobleach under such low-salt conditions.

At higher ionic strengths the situation is considerably more complex, for the following reason. With increasing ionic strength, not only do the relative populations of the different intercalation sites shift but also the longest-lived fluorescent component, which still dominates the photobleaching, moves from an intercalated site to an outside bound site. The latter site exhibits a somewhat shorter fluorescence lifetime (430 ps) and a much greater amplitude of rapid local angular motion, which reduces its anisotropy to about 24% of its initial value with a relaxation time of ~100 ps.[12] In contrast, at the lowest ionic strength examined previously (8.3 mM), rapid dye wobble relaxes the anisotropy of the longest-lived (630 ps) component only slightly to about 73% of its starting value with a relaxation time of ~200 ps.[12] In fact, the observed residual anisotropy after relaxation by rapid dye wobble declines progressively with increasing ionic strength from $(0.73) \times (2/5)$ at 8.3 mM to $(0.24) \times (2/5)$ at 207 mM.[12] Because both the equilibrium orientation and distribution of excursion angles of the outside bound dye are not yet known, it is not possible to interpret the *full* anisotropy decay at any but the very lowest ionic strengths (4 and 8 mM) of the present study. Although the equilibrium orientation and distribution of excursion angles of MB strongly affect the *amplitude*, they do not affect the *rate* of the *final* exponential decay of the optical anisotropy due to end-over-end tumbling. Thus, for the present purpose of determining the end-over-end rotational diffusion coefficients, the details of the equilibrium orientation and wobble of the dye are unimportant, provided that sufficient amplitude of the anisotropy remains to provide adequate signal in the tail of the anisotropy decay curve.

The samples are deoxygenated by bubbling argon saturated with buffer vapor through the solutions for 12−18 h prior to each experiment. The argon is also blown gently across the top of each sample during the experiments.

The sample cuvette is 1 mm thick by 1 cm in breadth by 4 cm deep. Stirring of the 300 μL sample in this narrow cuvette (to ameliorate any effects of transient heating and permanent photobleaching) is accomplished by periodically slowly withdrawing and reinjecting a small portion of the sample using a semicollapsible tube that is immersed in the sample at one end and at the other end contains an upstream N_2 bubble that is alternately pinched and released by a peristaltic pump.

The Transient Polarization Grating Method. A new transient polarization grating (TPG) instrument was constructed to perform these measurements. A detailed description is provided elsewhere,[9,13] so only a brief account will be given here. The grating is written in the sample by intersecting two coherent (0.04 cm^{-1} bandwidth) pulses (5 ns) of horizontally propagating laser light (690 nm), which have *orthogonal* (vertical and horizontal) polarizations. Each beam is about 2 mm in diameter and makes an angle $\theta/2 = 20°$ with respect to the grating normal. As a consequence of this excitation, the sample is uniformly bleached by approximately 1%. This is the fraction of MB molecules that undergo intersystem crossing to their triplet states, from which they return to the ground state with a relatively long lifetime of ~10−20 μs in these deoxygenated solutions. The repetition rate of this experiment is 10 s^{-1}. Although the intensity of the superimposed excitation pulses is uniform across the sample, the polarization of the light varies periodically from right circular to linear (polarized at $+\pi/4$ from vertical) to left circular to linear (polarized at $-\pi/4$ from vertical) and then back to right circular to begin another period. The regions of the sample that experience circular polarization undergo isotropic (unpolarized) photobleaching in the plane of the grating, whereas those that experience linear polarization undergo anisotropic photobleaching. That is, in the linear polarization regions, those intercalated MB molecules with transition dipoles aligned along the local polarization of the light are preferentially excited and become proportionately trapped in their triplet states. Because the MB triplet absorbance is negligible in the spectral region of the $S_0 \rightarrow S_1$ absorption band, those molecules are effectively bleached for the duration of their lifetime in the triplet state. In these experiments, the triplet state serves merely as a temporary reservoir for optically silent molecules. Because of the anisotropic photobleaching induced in the zones of linear polarization, the sample becomes uniaxially dichroic in those regions with symmetry axes alternately at $+\pi/4$ and $-\pi/4$ from vertical, as one moves along the grating. The excitation pulse energy (~0.2 mJ) is adjusted so that a MB

molecule with its transition dipole aligned along the local polarization in a linearly polarized region is cycled through its $S_0 \rightarrow S_1$ transition about 10 times during the pulse, when it fails to reach its triplet state. Consequently, MeBl molecules typically absorb several photons from the same pulse, which internally convert, before absorbing the one that leads to T_1. A noteworthy feature of the polarization grating is that the uniform intensity creates *no* ordinary thermal phase grating. Relaxation of such a phase grating by thermal diffusion would take place on the microsecond time scale of interest and substantially complicate the data analysis.

The amplitude of the photoinduced dichroism grating is monitored by diffraction of a CW, horizontally propagating, vertically polarized, 632.8 nm probe beam from a He−Ne laser. The angle (ϕ) of incidence of the probe beam and exit of the diffracted beam with respect to the grating normal satisfies the Bragg condition,

$$\sin \phi = \frac{632.8}{690.0} \sin (\theta/2) \tag{1}$$

so that $\phi = 18.3°$. The intensity of diffracted probe light is proportional to the square of the amplitude of the dichroism grating in the sample, and its polarization is rotated to horizontal.[14]

By writing the grating with 690 nm pulses and probing with a 632.8 nm beam and using appropriate narrow band-pass filters, we have effectively screened out the vast majority of scattered 690 nm light and also the MB fluorescence,[9,13] which is very short-lived (≤630 ps).[12] The 90° rotation of the polarization of the probe beam upon diffraction allows effective discrimination against the predominantly polarized scattered light by use of a polarizer in the detection optics. That same polarizer also eliminates polarized probe light that is diffracted from any adventitious weak thermal phase grating, such as might arise from the very small induced circular dichroism of the intercalated MB.[29]

The diffracted probe light is detected by single-photon counting via a photomultiplier and constant fraction discriminator (CFD). The output of the CFD is a nuclear instrumentation module (NIM) standard negative logic pulse of adjustable width, which is set to match the channel width (10 ns) of a transient digitizer−recorder, whose track and hold circuit samples once every 10 ns channel. In this way, every photon detected by the photomultiplier is captured (provided that the maximum count rate does not exceed 0.01 photons/10 ns) and stored in the appropriate recorder channel. Because the dichroism in the sample is monitored by a single detector, both systematic and random errors are significantly reduced compared to experiments in which the dichroism is detected by using two detectors. In particular, systematic errors due to any mismatch in the calibration of the two detectors are completely eliminated, which is crucial for obtaining precise data from the very tail of the decay curve.

The (slow) kinetics of photobleach recovery are measured by blocking one of the excitation pulses (so no grating is created) and monitoring the intensity of transmitted probe light, which is polarized at 54.7° from vertical for these measurements. This is done using a photodiode and the same transient recorder. The diffraction and absorbance signals are transferred to a computer and accumulated between successive shots. Typically, the responses to 50 000−100 000 shots are accumulated to provide adequate diffracted signals, but only 1000 accumulated shots are needed to produce excellent triplet decay curves.[13]

Least-squares fitting of the transient absorption curves to a double-exponential function typically yields a triplet decay function ($f_T(T)$) consisting of a major component with a lifetime ~10−20 μs and a minor component with much longer lifetime, ~70 μs. Because the kinetics of photobleach recovery are rather slow compared to the decay of the diffracted signal, and the precision of the $f_T(t)$ data is so great, the determination of $f_T(t)$ contributes negligibly to the error in our final results.

Rotations of the transition dipoles of the unbleached MB molecules toward the bleached orientations diminish the local dichroism and cause a decay of the diffracted signal. Likewise, decay of the triplet T_1 states of the bleached molecules back to their ground S_0 states also diminishes the dichroism and diffracted signal. In our experiment, the decay of the pure diffracted signal is given by[14,15]

$$S(t) = W[r(t)\, f_T(t)]^2 \tag{2}$$

where W is an unknown proportionality constant, $r(t)$ is the optical anisotropy, and $f_T(t)$ is the normalized triplet decay function. Translational diffusion generally also contributes to the decay of $S(t)$, but in the present experiments on 200 bp DNA/MB complexes, relaxation of the grating by translational diffusion is several hundred times slower than by end-over-end tumbling, so it can be omitted from the data analysis with negligible error. It is shown elsewhere that a heterodyne term involving diffracted light and a very small amount (1 part in 1000 of intensity) of horizontally polarized scattered probe light (probably from some imperfection in the cuvette surface) in fact averages to zero, presumably due to shot-to-shot variations in optical paths of the excitation pulses and consequent variations in both grating phase and phase of the diffracted light relative to that of the scattered light.[9,13] The homodyne and heterodyne terms were originally expected to have comparable amplitudes in the tail of the decay, in part because the heterodyne term decays half as fast as the homodyne term, but in fact the best-fit amplitude of the heterodyne term *in the tail of the accumulated signal* was always negligibly small compared to that of the homodyne term and had the size (and variable sign) expected from random noise in the data. The heterodyne term is clearly averaged to zero *in the accumulated signal*, although on any given shot it is almost certainly nonvanishing.

Theory

Data Analysis. The optical anisotropy, which governs the decay of either the fluorescence polarization anisotropy (FPA) or the transient photoinduced dichroism within the transient polarization grating, is given for a filament with mean local cylindrical symmetry by[15,16]

$$r(t) = (2/5)\mathrm{ARF} \sum_{n=0}^{2} I_n F_n(t)\, C_n(t) \tag{3}$$

wherein ARF is an amplitude reduction factor due to rapid isotropic wobble of the dye in its binding site,[16,17] the I_n are well-known trigonometric factors,[15−17] and $F_n(t) = \langle \exp[-(6 - n^2)\langle\Delta_x(t)^2\rangle/2]\rangle$ and $C_n(t) = \langle \exp[-n^2\langle\Delta_z(t)^2\rangle/2]\rangle$ are the tumbling and twisting correlation functions, respectively, averaged over all intercalation sites in the molecule. The quantities $\langle\Delta_x(t)^2\rangle$ and $\langle\Delta_z(t)^2\rangle$ are the mean-squared angular displacements of a subunit of the filament around its local body-fixed transverse and symmetry axes, respectively, at time t. The $\langle\Delta_x(t)^2\rangle$ contains a term, $2D_R t$, that increases in proportion to t, as well as a term due to bending deformations that reaches a finite plateau value at long times. Likewise, $\langle\Delta_z(t)^2\rangle$ contains a term, $2D_{\|} t$, that increases in proportion to t, as well as a term due to twisting deformations that reaches a finite plateau value at long times. Note that $C_0(t) = 1.0$ is actually a constant. For a long thin molecule, such as a 200 bp DNA, $D_{\|} \gg D_R$, so $C_1(t)\, F_1(t)$ and $C_2(t)\, F_2(t)$ relax much more rapidly than $C_0(t)\, F_0(t)$, which then becomes the prevailing term at long times in the tail of $r(t)$. Because the uniform azimuthal spinning and bending normal modes all relax much (≥10-fold) faster than end-over-

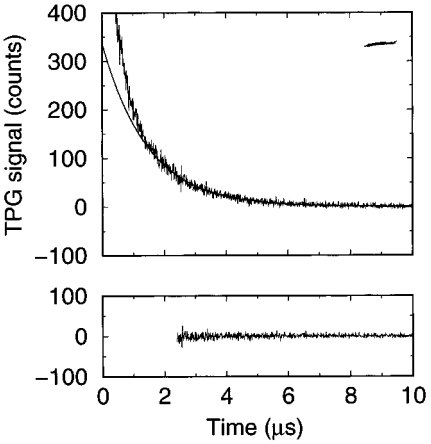

Figure 1. TPG signal $S(t)$ vs time for 200 bp DNA/MB complexes at 4 mM ionic strength. Data were collected for 120 000 shots. Sample contained 1.5 mg/mL DNA in 5 mM Tris, pH 7.5, at 294 K. The smooth line is the best-fit single-exponential decay over the time range from 2.4 to 10.0 μs. $S(t)$ was fitted by a single-exponential decay according to eq 4. Beginning at times greater than $t = 2.4$ μs the tail was fitted well with an end-over-end rotational relaxation time, $\tau_R = 4.26$ μs. The bottom panel shows the differences between experimental data and the best-fit curve.

end tumbling, at sufficiently long times $r(t)$ becomes a single-exponential decay,

$$r(t) = (2/5)\mathrm{ARF}I_0D_0(\infty)\exp[-6D_Rt] = M\exp[-6D_Rt] \quad (4)$$

wherein the prefactors have been lumped into a single amplitude factor M. Analytical approximations for $D_0(\infty)$ are given elsewhere[16,18,19] but are not needed here, since only the terminal exponential relaxation *rate*, $6D_R$, is desired. In the TPG method, the proportionality constant W between the diffracted signal and the magnitude of the maximum dichroism in the sample is not known. Instead, it is an additional unknown factor in the data analysis, which can be determined by fitting. However, knowledge of W is not necessary to determine D_R. Consequently, fitting here is carried out using

$$S(t) = A[\exp(-t/\tau_R)f_T(t)]^2 \quad (5)$$

where $\tau_R = (6D_R)^{-1}$ is the rotational relaxation time, $f_T(t)$ is the appropriate normalized photobleach recovery (or triplet decay) function, and A is an adjustable constant. The results of fitting the complete anisotropy decay, including fluorescence polarization anisotropy (FPA) data for DNA/ethidium complexes from 0 to 120 ns and TPG data for DNA/MB complexes from 20 ns to 10 μs, to determine the dynamic bending rigidity will be presented elsewhere.

The protocol adopted here is to fit the tail of $S(t)$ from different beginning times, $t_B \geq 1$ μs, to a final time of 10 μs. A typical fit is shown in Figure 1. There is no evidence of nonexponential decay in the very tail of the curve. With increasing t_B, the best-fit values of τ_R rise to a plateau, which is fairly constant from $t_B = 2.4$ to 3.4 μs or from 2.2 to 3.2 μs, depending on ionic strength, as shown in Figure 2. Beyond $t_B \simeq 3.5$ μs, errors in the plateau value increase. The best-fit values of τ_R under different conditions are taken from least-squares fits of horizontal lines to the data from $t_B = 2.4$ to 3.4 μs at the lower ionic strengths and 2.2 to 3.2 μs for ionic strengths $\gtrsim$14 mM.

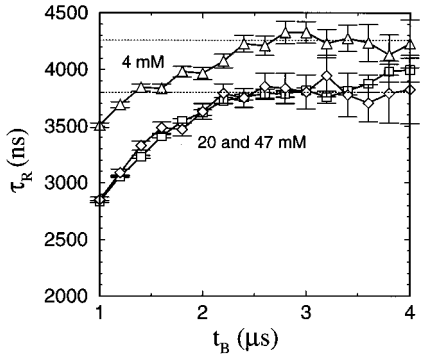

Figure 2. Best-fit end-over-end tumbling decay time (τ_R) for 200 bp DNA/MB complexes vs beginning time of the fit (t_B). The best-fit τ_R values remains relatively constant over the plateau regions from 2.40 to 3.40 μs for the 4 mM ionic strength data or from 2.20 to 3.40 μs for the 20 and 47 mM ionic strength data. At shorter times, faster components in the TPG signal (or the actual $r(t)$) cause τ_R to decrease with progressively shorter beginning times of the fitted data. At longer beginning times, τ_R starts to vary erratically with that beginning time. The best-fit horizontal lines obtained for the respective plateau regions correspond to $\tau_R = 4260 \pm 40$ for the 4 mM ionic strength data, $\tau_R = 3800 \pm 50$ for the 20 mM ionic strength data, and $\tau_R = 3780 \pm 30$ for the 47 mM ionic strength data.

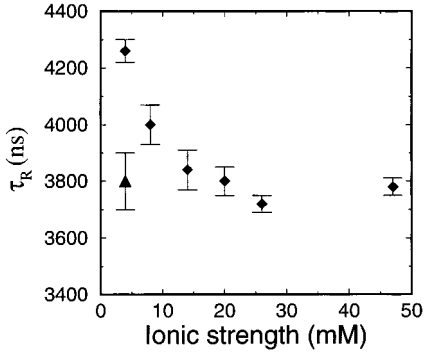

Figure 3. Best-fit end-over-end tumbling decay time (τ_R) for 200 bp DNA/MB complexes vs ionic strength. Diamonds correspond to 1.5 g/L (2.3 mM bp) DNA, while the triangle corresponds to the sample with 0.75 g/L (1.15 mM bp) DNA.

Table 1. Rotational Relaxation Times (τ_R) and Self-Rotational Diffusion Coefficients ($D_R = (6\tau_R)^{-1}$) for 200 bp DNA at pH 7.5 at 21 °C

[DNA] (g/L)	ionic strength[a] (mM)	τ_R (ns)	$D_R \times 10^{-4}$ (s^{-1})
1.5	4	4260 ± 40	3.91 ± 0.04
1.5	8	4000 ± 70	4.17 ± 0.07
1.5	14	3840 ± 70	4.34 ± 0.08
1.5	20	3800 ± 50	4.39 ± 0.06
1.5	26	3720 ± 30	4.48 ± 0.04
1.5	47	3780 ± 30	4.41 ± 0.04
0.75	4	3800 ± 100	4.39 ± 0.12

[a] Added ionic strength, excluding all counterions supplied by the DNA.

Results and Discussion

General Observations. The best-fit values of τ_R are plotted vs ionic strength of *added* electrolyte in Figure 3. These τ_R values and their corresponding self-rotational diffusion coefficients, $D_R = (6\tau_R)^{-1}$, are listed in Table 1. Neither the phosphate charges (4.6 mM) nor their counterions (4.6 mM) are included in the stated

Table 2. Effective Diameters, Second Virial Coefficients, and Second Virial Terms

L (Å)	I_{dia} (M)[a]	I_{dia}^{cor} (M)[b]	I_{add} (M)	d_B (Å)[c]	$B_2 \times 10^7$ (cm^3)[d]	ρB_2
510	50	48		76	2.47	0.22
680			47	76	4.00	0.27
510	16	14		132	5.50	0.50
680			20	112	6.75	0.46
510	5	3		260	16.1	1.46
680			4	245	22.4	1.53

[a] Ionic strength against which 1.5 g/L DNA solution was dialyzed by Fulmer et al.[3] [b] Ionic strength corrected for Donnan effect according to $I_{dia}^{cor}/I_{dia} = (1 + y^2)^{1/2} - y$, where $y = 2c_{bp}/2I_{dia}$, where c_{bp} is the concentration of bp, and all ions are assumed to be univalent. [c] Taken or interpolated from Table 1 of Stigter.[21] [d] Calculated according to eq 33 of Odijk,[22] which contains an electrostatic end effect analogous to a spherical cap end effect for hard rods.

ionic strengths, which correspond to added ions only. The rotational relaxation time *increases* significantly with decreasing ionic strength from 20 to 4 mM. Reducing the DNA concentration by 2-fold in the same 4 mM ionic strength buffer practically eliminates this effect of the decrease in ionic strength. Evidently, the observed effect of decreasing ionic strength on τ_R arises from *intermolecular* interactions, rather than from intramolecular effects such as enhanced electrostatic straightening or electrolyte friction.[1,2]

The upswing in τ_R between 20 and 4 mM ionic strength for our 200 bp DNAs falls in the same range as the decrease in scattered intensity observed by Fulmer et al. for their 150 bp DNAs.[3] The question arises whether the present 200 bp DNAs and the 150 bp DNAs of Fulmer et al.[3] are actually in corresponding states in their transition regions. It is frequently assumed that rodlike species of different length are in corresponding states in their different solutions when they exhibit identical second virial terms, ρB_2, where ρ (molecules/cm^3) is the rod number density and B_2 (cm^{-3}) is the second virial coefficient under the prevailing conditions. For example, the isotropic-to-nematic phase transition exhibited by neutral hard cylinders is predicted to begin when $\rho B_2 = 3.34$ and to end when $\rho B_2 = 4.48$, regardless of the cylinder length, provided the axial ratio is sufficiently great.[20,21]

B_2 is calculated for a pair of infinitely dilute charged rods in a solution containing the *added* ionic strength ($I_{add}(M)$) of the solution in question. In fact, Fulmer et al. did not simply add or mix extraneous ions with their DNA but instead dialyzed their DNA against solutions (containing mainly NaCl) at the stated ionic strengths (I_{dia}). Because of the Donnan effect, neutral salt is excluded somewhat from their polyion solutions. Hence, the I_{dia} values are corrected here to obtain the prevailing ionic strengths of *added* ions in those DNA solutions by using standard Donnan theory,

$$I_{dia}^{cor}/c_s = (1 + y^2)^{1/2} - y \qquad (6)$$

where $y = 2c_{bp}/2c_s$ is one-half the ratio of the concentration of polyion charge inside the DNA solution to concentration of univalent salt (c_s) in the dialyzate outside the DNA solution, and c_{bp} is the concentration of base pairs. It is assumed here that $c_s = I_{dia}$. Both I_{dia} and I_{dia}^{cor} are listed for three different ionic strengths in Table 2. At $I_{dia} = 50$, 16, and 5 mM ionic strength, the Donnan correction is to reduce I_{dia} by about 2 mM. Second virial coefficients are calculated according to the expression[22]

$$B_2 = \frac{\pi}{4} L^2 d_B (1 + 4d_B/L) \qquad (7)$$

where L is the rod length and d_B is the *effective* diameter of the rod. Equation 7 was derived by Odijk[22] and contains the classical result discussed by Onsager[20] and Stigter[21] plus an end-effect correction (the second term in parentheses) that is analogous to the spherical end-cap correction for hard cylinders. The d_B values are taken directly or interpolated/extrapolated from Table 1 of Stigter.[21] The interpolation/extrapolation was performed by first plotting Stigter's d_B values vs $1/c_s$, where c_s is the prevailing NaCl concentration, which yields a gently curving line. The d_B values relevant to the present ionic strengths are presented in our Table 2, along with the computed second virial coefficients, and the second virial terms, ρB_2, which appear in the final column. The 150 bp DNA of Fulmer et al. has $L = 510$ Å, and our 200 bp DNA has $L = 680$ Å; these lengths are indicated for the appropriate solutions in Table 2. Although both DNAs are present at 1.5 g/L, the rod number densities are $\tau = 9.09 \times 10^{15}$ and 6.82×10^{15} for the 150 and 200 bp DNAs, respectively. The ρB_2 term is 0.50 for the 150 bp DNA in $I_{dia}^{cor} = 14$ mM and 0.46 for the 200 bp DNA in $I_{add} = 20$ mM, so the two DNAs are in nearly corresponding states at these respective ionic strengths. The ρB_2 term rises almost 3-fold to 1.46 for the 150 bp DNA in $I_{dia}^{cor} = 3$ mM and to 1.53 for the 200 bp DNA in $I_{add} = 4$ mM, so the two DNAs are again in nearly corresponding states under these conditions. The largest (1.9-fold) decrease in scattered intensity of the 150 bp DNA in the study of Fulmer et al. occurred between $I_{dia} = 16$ and 5 mM (or $I_{dia}^{cor} = 14$ and 3 mM), whereas the rise in τ_R in the present study takes place between $I_{add} = 20$ and 4 mM, and in both cases ρB_2 increases from about 0.5 to 1.5. Thus, both phenomena appear to be associated with the same kind of intermolecular structural transition in solution. Unfortunately, we did not have sufficient 200 bp sample to undertake scattering experiments and could not confirm this conclusion directly by experiment.

The structural transition observed for the present 200 bp DNAs at low ionic strength appears *not* to be an isotropic-to-nematic phase separation of the type predicted by Onsager.[20] The present 4 mM solutions were examined extensively under a polarizing microscope, and no evidence of anisotropic phases was found. The overall intensity of light transmitted through the sample was uniform and equal to that of pure water in an identical cuvette. The microscope's magnification would have allowed detection of anisotropic domains as small as 10 μm, if they were in fact present.

Effects of Intermolecular Interactions on τ_R. Although the write pulses excite the entire collection of transition dipoles in the sample in a coherent manner, the collective excitations are almost immediately localized in a stochastic manner onto individual MB molecules. The subsequent absorption of probe light to assess the residual photoinduced dichroism likewise proceeds in a stochastic manner. As a consequence, the optical anisotropy $r(t)$ in eqs 2 and 3 is a *self-*, rather than a *mutual-*, correlation function, namely $r(t) = (2/5)4\pi\langle Y_{20}(\Omega_j(0))\, Y_{20}(\Omega_j(t))\rangle$, where $\Omega_j(t)$ is the instantaneous

solid angle of the transition dipole of the jth MB molecule and $Y_{20}(\Omega_j(t))$ is the indicated spherical harmonic function of $\Omega_j(t)$.[1,16] The absence of cross terms between different dye molecules is the signature of a *self*-correlation function. Hence, the measured $D_R = {}^1/_6\tau_R$ are *self*-rotational diffusion coefficients. The $r(t)$ that describes the decay of the photoinduced dichroism pertains to a fictitious collection of unbleached *copies* of the photobleached DNA molecules. The present TPG experiments are performed with one MB molecule per 100 bp, and slightly less than 1% of those become trapped in their triplet states. Consequently, less than 1 in 50 DNA molecules is labeled with a *bleached* chromophore. Hence, the orientations and rotations of the bleached DNAs, or equivalently of their unbleached copies, are largely uncorrelated with each other, apart from their initial polarized photoselection, so any cross terms in their rotational diffusion coefficients would be negligible, even if they were present. In a mutual rotational diffusion measurement, every molecule of interest is coherently excited and contributes in a coherent way to the observed signal, so the presence of signal necessarily implies some net alignment of the entire set of interacting molecules in the laboratory frame. Direct forces between any given aligned molecule and its net aligned neighbors then bias the Brownian motion to either enhance or retard its rotational relaxation and thereby affect the rate of decay of the overall alignment. However, in a *self*-rotational diffusion measurement, direct forces between a given aligned (bleached) molecule and its neighbors have no average effect to either enhance or retard its rotational diffusion, since their effects are unbiased (i.e., half the time acting in opposite directions). The observation of *self*-rotational diffusion coefficients is a very important feature of our experiment that distinguishes the present results from those that would be obtained by transient electric birefringence or dichroism or depolarized dynamic light scattering experiments, all of which yield *mutual* rotational diffusion coefficients.

Although intermolecular electrostatic interactions do not *directly* affect self-rotational diffusion, they do so *indirectly* via hydrodynamic interactions, which depend on positional and orientational pair correlations between the observed molecule and its neighbors. A useful measure of the strength of the direct interactions is the second virial term, ρB_2. For our 200 bp sample at 47 mM ionic strength, $\rho B_2 = 0.27$. Under such conditions, the virial series for the osmotic pressure, $\pi = \rho kT(1 + B_2\rho + B_3\rho^2 + ...)$, should converge uniformly and relatively quickly, and interactions between nearest-neighbor *pairs* should dominate the nonideality arising from electrostatic interactions. In this case, the mean-field electrostatic interactions favor *perpendicular* configurations of nearest neighbors over parallel configurations. This circumstance should prevail, albeit with stronger interactions, as the ionic strength is decreased to 26 mM, where $\rho B_2 = 0.37$. The hydrodynamic interactions pertinent to self-rotational diffusion diminish with increasing population of nonplanar perpendicular orientations of nearest neighbors, as shown below. Consequently, one might expect a slight increase in D_R, or decrease in τ_R, as the ionic strength is decreased from 47 to 26 mM. Although such a slight decrease in τ_R is consistent with our data, the statistical precision of the data is insufficient to support a firm conclusion in that regard.

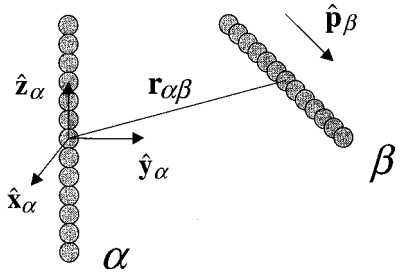

Figure 4. Two DNA molecules, α and β, are represented as a linear chain of contiguous beads of radius a. Vector $\mathbf{r}_{\alpha\beta}$ connects the center of mass of one molecule to the other, while $\hat{\mathbf{p}}_\beta$ is a unit vector along the β DNA molecule; $\hat{\mathbf{x}}_\alpha$, $\hat{\mathbf{y}}_\alpha$, $\hat{\mathbf{z}}_\alpha$ are unit vectors of the Cartesian coordinates positioned in the center of mass of molecule α, such that vector $\hat{\mathbf{z}}_\alpha$ is along α and $\hat{\mathbf{y}}_\alpha$ is oriented in such a way that $\hat{\mathbf{r}}_{\alpha\beta}$ lies in the $y-z$ plane.

As the ionic strength is decreased further from 20 to 4 mM, ρB_2 increases nearly 3-fold from 0.46 to 1.53, at which point the virial series for the osmotic pressure is no longer uniformly convergent. The third virial term, $\rho^2 B_3$, can be estimated using a formula proposed by Odijk,[22] which neglects end effects,

$$B_3 \cong \left(\frac{\pi}{4} L^2 d_B\right)^2 4\,\frac{d_B}{L} \tag{8}$$

Equation 8 is expected to underestimate the actual B_3. For the 200 bp DNA in 20 mM ionic strength, we have $\rho B_2 = 0.46$ and $\rho^2 B_3 \cong 0.06$, which confirms the predominance of the second virial term in that case. However, for the 200 bp DNA in 4 mM ionic strength, we have $\rho B_2 = 1.53$ and $\rho^2 B_3 = 0.56$, so higher-order interactions now make a substantial contribution to the nonideality of the solution. As will be shown below, the rise in τ_R suggests that the higher-order interactions act to promote more *parallel* alignment of the DNAs.

The self-rotational diffusion coefficient (D_R) depends on intermolecular distances that are relevant for hydrodynamic interactions and is unaffected by direct interactions, except for their influence on the distribution of such distances. Consequently, we do not expect identical D_R or τ_R values for *different* concentrations of DNA at those ionic strengths where their ρB_2 values match, because their intermolecular distances are still very different.

Analysis in Terms of Hydrodynamic Interactions. The end-over-end rotational relaxation time for self-diffusion is given by

$$\tau_R = (6D_R)^{-1} = f_R^{eff}/6kT \tag{9}$$

where f_R^{eff} is the effective friction factor, k is Boltzmann's constant, and T is the absolute temperature. An expression for f_R^{eff} will be developed using a dissipation argument, which is based on an approximate theory of the hydrodynamic coupling between a rotating labeled DNA rod (α) and an unlabeled neighboring DNA rod (β), which are illustrated in Figure 4. The hydrodynamic interactions are treated only to lowest order, so just two-body hydrodynamic interactions are considered. Such a treatment should be adequate for the relatively slight (12%) increase in τ_R and f_R^{eff} observed here. It will be shown in eq 18 that f_R^{eff} is equal to the unperturbed

value (f_R°) for an isolated DNA rod plus a contribution due to interactions of the rotating rod α with its neighbors.

The rods α and β are each subdivided into N (odd) beads. A coordinate frame $\mathbf{x}_\alpha$, $\mathbf{y}_\alpha$, $\mathbf{z}_\alpha$ is fixed in α with its origin on the central bead, and the unit vector $\hat{\mathbf{z}}_\alpha$ is taken along the rod axis. The central bead of β is located at $\mathbf{r}_{\alpha\beta}$ in the frame of α, and the unit vector $\hat{\mathbf{p}}_\beta$ runs along the rod axis of β. A particular bead on α is denoted by the index m, which takes the integral values, $-(N-1)/2$, $-(N-1)/2+1$, ... -1, 0, 1, ... $+(N-1)/2$, and increases in the direction of $\hat{\mathbf{z}}_\alpha$. A particular bead on β is denoted by the index n, which takes the corresponding integral values increasing in the direction of $\hat{\mathbf{p}}_\beta$. The vector $\mathbf{r}_{mn}$ from the mth bead on α to the nth bead on β can be written as

$$\mathbf{r}_{mn} = -2ma\hat{\mathbf{z}}_\alpha + \mathbf{r}_{\alpha\beta} + 2na\hat{\mathbf{p}}_\beta \tag{10}$$

wherein a is the bead radius. When the rod α rotates with angular velocity ω around a transverse axis, the *linear* velocity of the mth bead is

$$\mathbf{u}_m = \boldsymbol{\omega} \times 2ma\hat{\mathbf{z}}_\alpha \tag{11}$$

The fluid velocity ($\mathbf{v}_m$) at the position of the mth bead is assumed to arise entirely from reflected hydrodynamic wakes that originate from the instantaneous *translation* of m as *a consequence of the end-over-end rotation*, $\boldsymbol{\omega}$, of rod α. Because the rotational friction of long rods (for end-over-end tumbling) arises essentially entirely from such rotation-induced translations, this should be a satisfactory way to include also the hydrodynamic interactions between rods. Hence,

$$\mathbf{v}_m = \sum_{n=1}^{N} \mathbf{T}_{mnm}\cdot\mathbf{u}_m = \sum_{n=1}^{N} \mathbf{T}_{mnm}\cdot(\boldsymbol{\omega} \times 2ma\hat{\mathbf{z}}_\alpha) \tag{12}$$

where $\mathbf{T}_{mnm}$ is the hydrodynamic interaction tensor,

$$\mathbf{T}_{mnm} = -\frac{15}{4}\frac{a^4}{r_{mm}^4}\hat{\mathbf{r}}_{mn}\hat{\mathbf{r}}_{mn} \tag{13}$$

and the carets denote unit vectors. $\mathbf{T}_{mnm}$ is the lowest-order nonvanishing hydrodynamic interaction tensor between two noninteracting beads, one of which (m) is translating and the other of which (n) is not fixed but is freely suspended in the fluid and moves with the perturbed fluid velocity at its position.[23−26] In the present case, any given n-bead is not entirely free to respond to the fluid velocity at its position, because it is connected to the remaining $N-1$ beads of the β-rod. However, the entire β-rod does respond in a kind of average way to the local fluid velocities at its constituent beads. By using eq 13, we have introduced an additional approximation, namely that substituting the actual hydrodynamic interactions between a pair of rods by the sum of hydrodynamic interactions between their constituent beads, which are regarded as freely suspended, does not alter the final qualitative conclusions. Indeed, we suspect that even the quantitative error from this approximation is rather modest. The contribution of hydrodynamic interactions between rods α and β to the rate of energy dissipation associated with rotation of the rod α is given by

$$D_{\alpha\beta}^{\mathrm{hyd}} = \sum_{m=1}^{N} f_T^\circ(|\mathbf{u}_m - \mathbf{v}_m|^2 - |\mathbf{u}_m|^2) = -2f_T^\circ\sum_{m=1}^{N}(\mathbf{u}_m\cdot\mathbf{v}_m) + O|\mathbf{v}_m|^2 \tag{14}$$

where $f_T^\circ = 6\pi\eta a$ is the translational friction factor of an isolated bead. The term of order $|\mathbf{v}_m|^2$ is neglected to obtain just the lowest-order effects of hydrodynamic interactions. Substituting eqs 12 and 13 into 14 yields

$$D_{\alpha\beta}^{\mathrm{hyd}} = 2f_T^\circ\sum_m\sum_n(\hat{\omega} \times 2ma\hat{\mathbf{z}}_\alpha)\cdot\mathbf{T}_{mnm}\cdot(\omega \times 2ma\hat{\mathbf{z}}_\alpha) \tag{15}$$

$$= 30f_T^\circ\omega^2a^6\sum_m\sum_n(\hat{\omega} \times \hat{\mathbf{z}}_\alpha\cdot\hat{\mathbf{r}}_{mn})^2\left(\frac{m^2}{r_{mn}^4}\right) \tag{16}$$

where $\hat{\boldsymbol{\omega}}$ denotes a unit vector along $\boldsymbol{\omega}$. The average total rate of energy dissipation associated with the rotation of rod α is then

$$D_\alpha^{\mathrm{tot}} = D_\alpha^\circ + \sum_\beta\langle D_{\alpha\beta}^{\mathrm{hyd}}\rangle = f_R^{\mathrm{eff}}\omega^2 \tag{17}$$

wherein $D_\alpha^\circ = f_R^\circ\omega^2$ is the contribution of the isolated rod, and the effective friction factor is

$$f_R^{\mathrm{eff}} = f_R^\circ + 30f_T^\circ a^6\sum_\beta\sum_m\sum_n\left\langle(\hat{\boldsymbol{\omega}} \times \hat{\mathbf{z}}_\alpha\cdot\hat{\mathbf{r}}_{mn})^2\left(\frac{m^2}{r_{mn}^4}\right)\right\rangle \tag{18}$$

where f_R° is the rotational friction factor of the isolated rod. The angular brackets in eq 18 denote an ensemble average over the equilibrium distribution of rod orientations and positions, plus another average over the distribution of angular velocities $\boldsymbol{\omega}$. The quantity $\hat{\mathbf{s}} \equiv \hat{\boldsymbol{\omega}} \times \hat{\mathbf{z}}_\alpha$ is a unit vector in a plane perpendicular to $\hat{\mathbf{z}}_\alpha$, and it must be averaged over all orientations in that plane in a uniformly weighted manner. When eq 10 is employed in eq 18, the term in angular brackets becomes

$$t_{mn} = \left\langle\frac{m^2}{r_{mn}^6}[\hat{\mathbf{s}}\cdot(-2ma\hat{\mathbf{z}}_\alpha) + \hat{\mathbf{s}}\cdot\mathbf{r}_{\alpha\beta} + \hat{\mathbf{s}}\cdot(2na\hat{\mathbf{p}}_\beta)]^2\right\rangle_{\mathbf{r}_{\alpha\beta},\hat{\mathbf{p}}_\beta}$$

$$= \left\langle\frac{m^2}{r_{mn}^6}\left(\frac{r_{\alpha\beta}^2}{3} + \frac{(2na)^2}{3} + 4nar_{\alpha\beta}\langle\hat{\mathbf{r}}_{\alpha\beta}\cdot\hat{\mathbf{s}}\hat{\mathbf{s}}\cdot\hat{\mathbf{p}}_\beta\rangle_{\hat{\mathbf{s}}}\right)\right\rangle_{\mathbf{r}_{\alpha\beta},\hat{\mathbf{p}}_\beta} \tag{19}$$

$$= \frac{m^2}{3}\left\langle\frac{r_{\alpha\beta}^2 + ((2na)^2 + 12nar_{\alpha\beta}\langle\hat{\mathbf{r}}_{\alpha\beta}\cdot\hat{\mathbf{s}}\hat{\mathbf{s}}\cdot\hat{\mathbf{p}}_\beta\rangle_{\hat{\mathbf{s}}})}{|-2ma\hat{\mathbf{z}}_\alpha + \mathbf{r}_{\alpha\beta} + 2na\hat{\mathbf{p}}_\beta|^6}\right\rangle_{\mathbf{r}_{\alpha\beta},\hat{\mathbf{p}}_\beta}$$

The subscripts $\hat{\mathbf{s}}$ on the interior angular brackets denotes a uniformly weighted average of $\hat{\mathbf{s}}$ over the plane perpendicular to $\hat{\mathbf{z}}_\alpha$. The subscripts $\mathbf{r}_{\alpha\beta}$,$\hat{\mathbf{p}}_\beta$ on the exterior angular brackets denote an ensemble average over the equilibrium distribution of lengths and orientations of inter-rod vectors, $\mathbf{r}_{\alpha\beta}$, and orientations, $\hat{\mathbf{p}}_\beta$, of the β-rod, when the α-rod has orientation $\hat{\mathbf{z}}_\alpha$. Changes in the t_{mn}, f_R^{eff}, and τ_R due to changes in the direct forces are considered next.

The mean-field electrostatic interactions between beads are repulsive and vary as $e^{-\lambda r_{mn}}/r_{mn}$, where λ is

the Debye screening parameter, so repulsions are strongest for the closest beads. Thus, increasing the strength of such repulsive interactions should diminish the relative weight of those configurations with the smaller $r_{\alpha\beta}$ (compared to the average inter-rod spacing), and for fixed $r_{\alpha\beta}$ should diminish the relative weights of those configurations in which either $\hat{\mathbf{z}}_\alpha$ or $\hat{\mathbf{p}}_\beta$, or both, are roughly parallel or antiparallel to $\hat{\mathbf{r}}_{\alpha\beta}$. These changes all diminish the relative weights of the t_{mn} terms with the smallest denominators and largest magnitudes and should thus lead to a *decrease* in f_R^{eff} (in eq 18) and τ_R. However, this is contrary to the observed increase in τ_R with decreasing ionic strength from 20 to 4 mM. What part of the distribution function is changing to increase some of the t_{mn} in eq 19, as well as f_R^{eff} and τ_R? As the relative weights shift with increasing repulsive interactions to favor configurations in which $\hat{\mathbf{z}}_\alpha$ and $\hat{\mathbf{p}}_\beta$ are more perpendicular to $\hat{\mathbf{r}}_{\alpha\beta}$, this could occur in either of two ways, namely (1) such that $\hat{\mathbf{z}}_\alpha$ is also more perpendicular to $\hat{\mathbf{p}}_\beta$ or (2) such that $\hat{\mathbf{z}}_\alpha$ and $\hat{\mathbf{p}}_\beta$ become more aligned (or antialigned) with each other. More perpendicular (nonplanar) orientations of adjacent rods (i.e., possibility (1)) are expected in the region of ionic strengths (47−26 mM), wherein the second virial term dominates and interactions with only a single neighbor are most important. With decreasing ionic strength in this region, $\hat{\mathbf{z}}_\alpha$ and $\hat{\mathbf{p}}_\beta$ should become more perpendicular to both $\hat{\mathbf{r}}_{\alpha\beta}$ and each other, so hydrodynamic interactions are diminished, and f_R^{eff} and τ_R should decrease slightly. This prediction is consistent with our data from 47 to 26 mM ionic strength. Possibility (2), in which the more aligned (or antialigned) orientations of side-by-side rods are favored, admits significantly enhanced hydrodynamic interactions, because *every* subunit of each rod experiences relatively strong hydrodynamic interactions with its neighboring rods. Indeed, this appears to be the only plausible change in the distribution of the $\hat{\mathbf{r}}_{\alpha\beta}$ and $\hat{\mathbf{p}}_\beta$ (at fixed $\hat{\mathbf{z}}_\alpha$) with increasing repulsive interactions that would act to enhance the hydrodynamic interactions. Thus, the observed increase in τ_R and f_R^{eff} with decreasing ionic strength from 20 to 4 mM strongly suggests that increasing repulsive interactions in this region favor parallel alignment of side-by-side neighbors, so that $\hat{\mathbf{z}}_\alpha$ and $\hat{\mathbf{p}}_\beta$ become more parallel to each other as they become more perpendicular to $\hat{\mathbf{r}}_{\alpha\beta}$. As noted previously, multirod interactions are important in this region of ionic strength. Moreover, multirod interactions are known to induce parallel alignment of neighboring rods and eventually even formation of a nematic phase. In fact, the magnitude of the second virial term, $\rho B_2 = 1.53$, in 4 mM ionic strength is only 2.2-fold smaller than the value (3.34) at which separation of an anisotropic phase is predicted to begin.[20]

Our proposed scenario for the effects of direct interactions on intermolecular structure and τ_R in our 1.5 g/L DNA samples is as follows. From 47 to 26 mM ionic strength, the effects of intermolecular interactions are manifested primarily between nearest-neighbor pairs, with the result that mutually perpendicular orientations of such pairs are favored. This change and the decline in pair configurations with short intermolecular distances act to decrease somewhat the strength of hydrodynamic interactions and thus to *decrease* slightly f_R^{eff} and τ_R. However, from 20 to 4 mM ionic strength, the effects of the steadily growing intermolecular forces become manifested increasingly in multirod interactions that favor configurations in which the rod and its neighbors become not only increasingly perpendicular to their inter-rod vectors but also more parallel (or antiparallel) to each other. This causes a significant increase in hydrodynamic interactions, in f_R^{eff}, and in τ_R. In brief, we attribute the rise in τ_R between 20 and 4 mM ionic strength to a change in orientation of nearest-neighbor rods from slightly more perpendicular to somewhat more parallel, which is driven by the onset of multirod interactions. This effect presumably arises mainly from multirod repulsive (excluded-volume) interactions, but an orientation-dependent attractive contribution from correlated longitudinal charge fluctuations[27,28] could also conceivably make a contribution.

As noted above, the 150 bp DNA sample of Fulmer et al.[3] over the range of ionic strengths, $I_{dia}^{cor} = 14-3$ mM, spans nearly the same range of corresponding states as our 200 bp DNA sample over the range $I_{add} = 20-4$ mM. Hence, the same kind of structural transition may be inferred for both samples. Thus, the splitting of the dynamic light scattering correlation functions for the sample of Fulmer et al.[3] into ordinary and extraordinarily slow modes, which is observed between $I_{dia}^{cor} = 14$ and 3 mM, is presumably associated with this same intermolecular structural transition.

Comparison with Rotational Diffusion Studies of Smaller RNAs and DNAs. End-over-end self-rotational relaxation times (τ_{Rs}) of a tRNA and different 12 and 16 bp duplex DNAs were investigated under various conditions by time-resolved fluorescence polarization anisotropy (FPA) of intercalated ethidium. The τ_{Rs} of the tRNA was found to remain constant, independent of tRNA concentration over the range $1 \times 10^{-5}-2 \times 10^{-3}$ M and independent of added ionic strength over the range 2−100 mM.[30] At the higher tRNA concentrations and lower ionic strengths (below 10 mM), these tRNAs interact so strongly that they are translationally ordered (as manifested by maxima in their small-angle X-ray scattering data, greatly reduced total intensity scattering of visible light, and the appearance of very slow components in their dynamic light scattering correlation functions),[31] yet their self-rotational diffusion proceeds in a completely unhindered manner. The effective axial ratio of this relatively short L-shaped molecule is presumably too small for it to exhibit the kind of cooperative orientational ordering exhibited by the present 200 bp DNA. In contrast, the τ_{Rs} of still smaller 12 and 16 bp DNAs in ∼100−200 mM ionic strength generally increase significantly, when the duplex concentration is raised from 2×10^{-5} to 3×10^{-3} M (B. S. Fujimoto, unpublished results).[32,33] However, such effects typically appear only at weight/unit volume concentrations (≥10 g/L) that are ∼10-fold larger, and molarities ($\geq 10^{-3}$ M) that are ∼100-fold larger, than that ($\sim 1 \times 10^{-5}$ M) of the 200 bp sample in the present study and most likely arise from a different mechanism, specifically from blunt-end association to form linear dimers. When the DNA concentration is sufficiently high ($\geq 5 \times 10^{-3}$ M), cross-peaks in the 2-D NOESY spectrum between the first and last base pairs in the sequence can in some cases be observed, which indicates directly the formation of linear dimers.[34] For DNA concentrations between 1×10^{-3} and 5×10^{-3} M, where the dimer/monomer concentration ratio is more modest (e.g., 0.185),[32,33] such NOESY cross-peaks are not evident, presumably because their amplitude is too low. Nevertheless, in this range the FPA data are significantly better fitted by a monomer−dimer equilibrium

model than by an enhanced uniform (effective) viscosity model, provided the DNA contains 16 or more bp (B. S. Fujimoto, unpublished results), so the presence of dimers can be indirectly inferred. For duplex concentrations much below 1×10^{-3} M, such experiments give no evidence of linear dimers. The dimerization constant apparently varies somewhat with sequence, as would be expected for an end-to-end association due to short-range attractive interactions (B. S. Fujimoto, unpublished results). Mutual rotational relaxation times (τ_{Rm}) were determined by depolarized dynamic light scattering studies of 12 and 20 bp DNAs. These, too, are independent of DNA concentration up to 10^{-3} M, but increase significantly, when the concentration is increased to higher levels,[35,36] and this increase in τ_{Rm} is enhanced by lowering the NaCl concentration from 100 to 10 to 0 mM.[36] These effects presumably also stem at least in part from the formation of linear dimers. In summary, tRNAs, which lack the blunt ends necessary to form dimers, do not significantly dimerize under any conditions, but linear duplex oligonucleotides with blunt ends can form detectable populations of linear dimers at sufficiently high concentration ($\geq 1 \times 10^{-3}$ M). In the case of the present 200 bp DNA, there is no evidence in the TPG signal of any very slow relaxation with time constant in the range ($\sim$32 μs) expected for linear dimers. The molarity (10^{-5} M) and weight/unit volume (1.5 g/L) of this 200 bp DNA are apparently too low (and its self-repulsions are possibly too great) to form a significant population of linear dimers. Certainly, there is no evidence that a significant population of linear dimers exists at duplex concentrations much below 10^{-3} M in this or any other system studied to date.

A Possible Connection to the Isotropic-to-Nematic Transition. What is the relation between the intermolecular structural transitions in these 150 and 200 bp DNA samples and the isotropic−nematic transition discussed by Onsager[20] and Stigter?[21] When Odijk's expression[22] is used for the second virial coefficient, the second virial term of either the 150 bp DNA of Fulmer et al. in 3 mM ionic strength, or the present 200 bp DNA in 4 mM ionic strength, is only a factor of $\sim$2.2-fold below the predicted *threshold* value ($\rho B_2 = 3.34$) for appearance of a nematic phase of neutral hard rods. In fact, the present sample exhibited no detectable nematic phase. Although Fulmer et al. extended their studies to 10-fold lower ionic strength ($I_{dia} = 5.6 \times 10^{-4}$ mM), where some nematic phase might have been expected, none was observed.[3] There are several reasons why the predicted threshold for neutral hard rods might not be simply applicable to 150−200 bp DNAs.

(1) The interaction potential between neutral hard rods does not vary as the rod concentration is varied from zero to its threshold value, where higher virial terms are important. However, the effective screened Coulomb interaction between charged rods inevitably varies with rod concentration, even when the suspension of rods is maintained in osmotic equilibrium with a solution of fixed small-ion concentration. It is well-known that the structure of a suspension of charged spherical colloids plus their counterions in a salt solution can be fairly accurately described by a one-component plasma model, wherein the effective interaction between colloids is a screened Coulomb potential. Intrinsic counterions and added salt ions both contribute to the screening parameter, which then increases with the concentration of charged colloids.[1,2] Consequently, in the case of charged rods the second virial coefficient, which is calculated for two infinitely dilute rods that interact via a screened Coulomb potential with a *fixed* screening parameter, may not provide the same guide to behavior of more concentrated rods as it does in the case of neutral hard rods. If account were taken of the increase in screening parameter with rod concentration, that would presumably shift the isotropic−nematic transition to still lower added ionic strength, or possibly eliminate it altogether, if a sufficiently low effective ionic strength could not be attained (e.g., due to the presence of intrinsic counterions).

(2) The effective axial ratios, L/d_B, decrease rapidly due to the rapid expansion of d_B with decreasing ionic strength and might be too small to admit a transition to the nematic phase. For the 150 bp DNAs at 1.5 g/L in 3 mM ionic strength, $L/d_B = 1.96$, and for the 200 bp DNAs at 1.5 g/L in 4 mM ionic strength, $L/d_B = 2.78$, neither of which may suffice to exhibit a nematic phase.

(3) A nematic phase coexisting with an isotropic phase would have a significantly higher density of charged rods. The resulting Donnan effect would act to decrease the concentration of added small ions (i.e., salt) in the nematic phase and increase it in the isotropic phase. Thus, the electrostatic free energy of the coexisting isotropic phase would be somewhat lower than reckoned by assuming a uniform distribution of added small ions between the two phases, and the electrostatic free energy of the nematic phase would be correspondingly higher. Hence, the transition would set in at a lower added ionic strength than predicted by the usual threshold criterion for hard rods, namely $\rho B_2 = 3.34$.

(4) Correlated longitudinal charge fluctuations on adjacent DNAs[27,28] may partially counter the effect of mean-field electrostatic repulsions to resist parallel rod orientations. Hence, the *net* repulsion may be significantly less than that predicted by mean-field theory. If this effect were significant, it would favor the nematic phase and shift the transition threshold to a higher ionic strength.

Given the various reasons to expect both a lower and a higher transition threshold, one might simply suspect that the intermolecular structural transitions manifested in the study of Fulmer et al. and in the present work correspond to a kind of thwarted isotropic to nematic transition. The transition could be thwarted by (1) too high an ionic strength from the intrinsic counterions alone, (2) too small an axial ratio, or (3) too large a Donnan effect on the partitioning of added small ions between the anisotropic and isotropic phases.

If the isotropic-to-nematic transition were thwarted by such a Donnan effect, the formation of a *macroscopic* nematic phase that significantly excludes added salt ions would be prevented (or at least put off). Nevertheless, small fluctuating clusters of aligned rods that retain a significantly higher concentration of salt ions in their interior could perhaps still exist as long-lived species in solution. The idea here is that a *macroscopic* phase retains in its interior essentially all of its intrinsic counterions, which are in turn responsible for salt exclusion. However, small clusters, which release a significant fraction of their intrinsic counterions into the ion atmosphere surrounding the cluster, may exhibit a lower mean intrinsic counterion concentration, and retain a significantly higher salt concentration in their interior, and therefore be more stable than the corresponding macroscopic phase. Such self-assembled lim-

ited clusters of aligned rods could conceivably be responsible for the extraordinarily slow components in the dynamic light scattering correlation functions of Fulmer et al.[3]

Acknowledgment. This research was supported in part by NSF grant MCB 9607344, and also in part by NSF grant PHY94-07194. The latter grant supported a visit by J.M.S. to the Institute of Theoretical Physics at the University of California at Santa Barbara, during which some of the present ideas were refined.

References and Notes

(1) Schurr, J. M.; Schmitz, K. S. *Annu. Rev. Phys. Chem.* **1986**, *37*, 271.
(2) Schmitz, K. S. *Macroions in Solution and Colloidal Suspension*; VCH Publishers: New York, 1993.
(3) Fulmer, A. W.; Benbasat, J. A.; Bloomfield, V. A. *Biopolymers* **1981**, *20*, 1147.
(4) Drifford, M.; Dalbiez, J.-P. *Biopolymers* **1985**, *24*, 1501.
(5) Odell, J. A.; Atkins, E. D. T.; Keller, A. *J. Polym. Sci., Polym. Lett.* **1983**, *12*, 289.
(6) Keep, G. T.; Pecora, R. *Macromolecules* **1985**, *18*, 1167.
(7) Levij, M.; De Bleijser, J.; Leyte, J. C. *Chem. Phys. Lett.* **1981**, *83*, 183.
(8) Shibata, J. H.; Schurr, J. M. *Biopolymers* **1979**, *18*, 1831.
(9) Naimushin, A. N. Ph.D. dissertation, University of Washington, 1999.
(10) Bergmann, K.; O'Konski, C. T. *J. Phys. Chem.* **1963**, *67*, 2169.
(11) Hagmar, P.; Pierrou, S.; Nielsen, P.; Nordén, B.; Kubista, M. *J. Biomol. Struct. Dyn.* **1992**, *9*, 667.
(12) Fujimoto, B. S.; Clendenning, J. B.; Delrow, J. J.; Heath, P. J.; Schurr, J. M. *J. Phys. Chem.* **1994**, *98*, 6633.
(13) Naimushin, A. N.; Fujimoto, B. S.; Delrow, J. J.; Schurr, J. M. *Rev. Sci. Instrum.* **1999**, *70*, 2471.
(14) Von Jena, A.; Lessing, H. E. *Opt. Quantum Electron.* **1979**, *11*, 419.
(15) Schurr, J. M. *Chem. Phys.* **1984**, *84*, 71.
(16) Schurr, J. M.; Fujimoto, B. S.; Wu, P.; Song, L. Fluorescence Studies of Nucleic Acids: Dynamics, Rigidities, and Structures. In *Topics in Fluorescence Spectroscopy;* Lakowicz, J. R., Ed.; Plenum Press: New York, 1992; Vol. 3, p 137.
(17) Schurr, J. M.; Fujimoto, B. S. *Biopolymers* **1988**, *27*, 1543.
(18) Wu, P. G.; Fujimoto, B. S.; Schurr, J. M. *Biopolymers* **1987**, *26*, 1463.
(19) Song, L.; Allison, S. A.; Schurr, J. M. *Biopolymers* **1990**, *29*, 1773.
(20) Onsager, L. *Ann. N. Y. Acad. Sci.* **1949**, *51*, 627.
(21) Stigter, D. *Biopolymers* **1977**, *16*, 1435.
(22) Odijk, T. *J. Chem. Phys.* **1990**, *93*, 5172.
(23) Murphy, T. J.; Aguirre, J. L. *J. Chem. Phys.* **1972**, *57*, 2098; **1972,** *59*, 1833.
(24) Batchelor, G. K. *J. Fluid Mech.* **1972**, *52*, 245.
(25) Montgomery, J. A.; Berne, B. J. *J. Chem. Phys.* **1977**, *67*, 4589.
(26) Allison, S. A.; Chang, E. L.; Schurr, J. M. *Chem. Phys.* **1979**, *38*, 29.
(27) Grønbech-Jensen, N.; Mashl, R. J.; Bruinsma, R. F.; Gelbart, W. M. *Phys. Rev. Lett.* **1997**, *78*, 2477.
(28) Ha, B.-Y.; Liu, A. *Phys. Rev. Lett.* **1997**, *79*, 1289.
(29) Nordén, B.; Tjernfeld, F. *Biopolymers* **1982**, *21*, 1713.
(30) Thomas, J. C.; Schurr, J. M.; Hare, D. R. *Biochemistry* **1984**, *23*, 5407.
(31) Patkowski, A.; Gulari, E.; Chu, B. *J. Chem. Phys.* **1980**, *73*, 4178.
(32) Nuutero, S.; Ribeiro, S.; Fujimoto, B. S.; Flynn, P. F.; Reid, B. R.; Ribeiro, N. S. *Biopolymers* **1994**, *34*, 463.
(33) Diaz, R.; Fujimoto, B. S.; Schurr, J. M. *Biophys. J.* **1997**, *72*, A322.
(34) Zhu, L.; Chou, S. H.; Reid, B. R. *J. Mol. Biol.* **1995**, *254*, 623.
(35) Eimer, W.; Williamson, J. R.; Boxer, S. G.; Pecora, R. *Biochemistry* **1990**, *29*, 799.
(36) Liu, H.; Skibinska, L.; Gapinsky, J.; Patkowski, A.; Fischer, E.; Pecora, R. *J. Chem. Phys.* **1998**, *109*, 7556.

MA990690V